Catalysis Letters (2021) 151:138–146
https://doi.org/10.1007/s10562-020-03280-2

Kinetic Effect of Surface Chemisorbed Oxygen on Platinum-Catalyzed Hydrogen Peroxide Decomposition

Rui Serra-Maia[1] · J. Donald Rimstidt[2] · F. Marc Michel[2]

Received: 14 April 2020 / Accepted: 1 June 2020 / Published online: 6 June 2020

Abstract

The chemical decomposition of H_2O_2 to H_2O and O_2 catalyzed by platinum nanocatalysts is important in many technologies such as steam propulsion, biosensors, fuel cells, and synthetic chemistry. Surface chemisorbed oxygen strongly impacts the kinetics of this reaction. However, the effect of this surface species has not been quantified in the context of the reaction mechanism. This study determined the rate constants of the elementary reaction steps of H_2O_2 decomposition on platinum nanocatalysts. For that, hydrogen peroxide decomposition rate measurements were analyzed on samples with variable surface chemisorbed oxygen (Pt(O)) abundance. The order of reaction in terms of surface Pt(O) abundance is 0.83, which indicates a nearly first order effect on the rate of H_2O_2 decomposition. This result is consistent with a reaction mechanism for H_2O_2 decomposition on platinum that involves two cyclic steps, where step 1 is the rate limiting step.

$$\text{Step 1}\quad Pt + H_2O_2 \xrightarrow{k=0.0028} H_2O + Pt(O)$$

$$\text{Step 2}\quad Pt(O) + H_2O_2 \xrightarrow{k=0.038} Pt + O_2 + H_2O$$

$$\text{Overall}\quad 2H_2O_2 \xrightarrow{k=0.037} O_2 + 2H_2O$$

The rate constant (k) of step 2 is 14 times higher than that of step 1 at a reaction temperature T = 295 K. This is consistent with a 4.4 time larger activation energy for step 1. Reaction rates are initially faster on samples with more surface Pt(O) sites because these sites decompose H_2O_2 through step 2 in the first cycle of the reaction. The relative rates of step 1 and step 2 become smaller at higher temperature. The method presented in this study can be used for determining the rate constants of the intermediate reaction steps of many other chemical reactions that are important for numerous scientific and technological applications.

Graphic Abstract

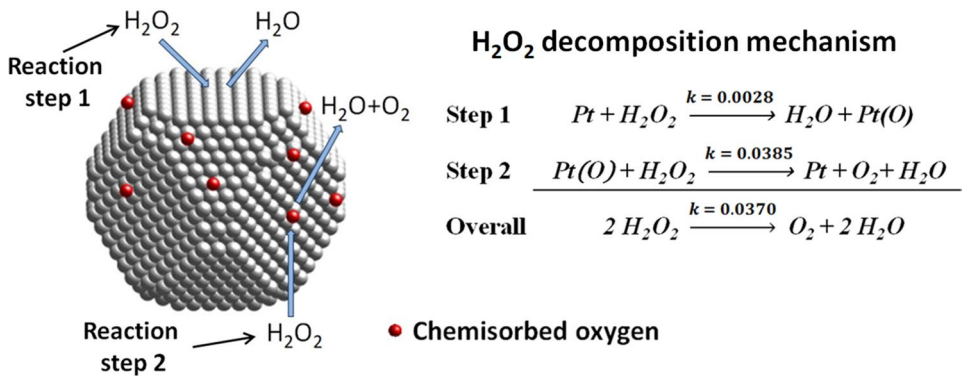

Keywords Kinetics · Rate constant · Chemisorbed oxygen · Rate-limiting step · Catalytic activity

✉ Rui Serra-Maia
ruism@seas.upenn.edu

Extended author information available on the last page of the article

1 Introduction

The decomposition of H_2O_2 to H_2O and O_2 catalyzed by platinum (Pt) nanocatalysts is an important chemical reaction in energy conversion, chemical synthesis, and biological applications, among others [1–8]. In hydrogen fuel cells, for example, H_2O_2 can form as a parasitic intermediate of the oxygen evolution reaction and then decompose to H_2O and O_2, which lowers the overall yield of the process [9–11]. Similarly, the decomposition of H_2O_2 at the catalyst surface prevents the accumulation of high concentrations of H_2O_2 during its synthesis, which results in significant economic losses [12, 13]. A catalytic coating was also recently implemented in super hydrophobic underwater surfaces to generate O_2 in situ from H_2O_2 to form a thin gas layer between the surface and water, which reduces drag and increases energy efficiency [14]. In addition to industrial applications, the decomposition of H_2O_2 by porous Pt nanoparticles is being used to enhance cancer treatments [15] and in other biomedical applications [16].

Hydrogen peroxide decomposition on platinum occurs via a two-step mechanism in which Pt oxidizes to Pt(O) with the release of a molecule of H_2O in the first step. In the second step Pt(O) reduces back to Pt releasing a second molecule of H_2O and molecular O_2 [17]. The environmental conditions and catalyst properties play a complex role in the rate and mechanism of the overall reaction [18]. The reaction is first order in terms of H_2O_2 concentration and is affected by temperature and pH [19–23]. Previous studies reported that the rate of H_2O_2 decomposition correlates with catalyst particle size [17, 19, 20, 24, 25]. However, we recently showed that the size effect is explained by a correlation between surface chemisorbed oxygen abundance and particle size on platinum nanocatalysts heated in air [26]. Calcination of the nanocatalysts in the presence of air increases the abundance of chemisorbed oxygen at the catalysts surface which increases the rate of H_2O_2 decomposition [17, 24, 27]. Understanding these effects is important because catalysts are subjected to a range of conditions before and during their use, which affect their physicochemical properties and therefore impact their catalytic rate of H_2O_2 decomposition.

The rate constants of the elementary reaction steps of H_2O_2 decomposition on platinum have never been quantified. This is important because the decomposition of H_2O_2 on platinum happens through a two-step process and one H_2O_2 molecule is decomposed in each step [17]. This opens the opportunity for catalyst improvements that target the rate limiting step of the reaction. It is thus crucial to evaluate the relative rate of each reaction step in order to control the overall rate of reaction.

In this study we quantify the rate constants of the intermediate reaction steps of H_2O_2 decomposition on platinum. For that, we investigated the effect of surface oxygen in the overall rate of reaction on platinum nanocatalysts subjected to different surface treatments. The results show that the first step of H_2O_2 decomposition involving $Pt \rightarrow Pt(O)$ is the rate limiting step of the reaction and is 14 times slower than the second step where $Pt(O) \rightarrow Pt$ along with the decomposition of a second molecule of H_2O_2. That is corroborated by a 4.4 times larger activation energy for step 1. This new information enables targeted catalyst optimization to improve our ability to control the rate of H_2O_2 decomposition catalyzed by platinum nanocatalysts in different applications.

2 Materials and Methods

2.1 Platinum Nanocatalysts

The rate of H_2O_2 decomposition for platinum nanocatalysts was analyzed as a function of their surface oxygen abundance. Rate data were obtained from the literature and normalized for surface area [17, 25, 26]. The surface chemisorbed oxygen abundance of the samples has the range of $0.21 < \theta < 0.69$ [26] (Table 1). The platinum nanocatalysts used in these prior studies are known as platinum black and platinum nanopowder. These two platinum nanomaterials are synthesized through different methods, which results in distinct surface chemisorbed oxygen abundance [25]. Platinum black is synthesized by reductive hydrogenation of PtO_2 (known as Adam's catalyst) in aqueous dispersion [28]. Platinum nanopowder on the other hand is obtained by chemical vapor deposition condensation [29]. Both samples were subjected to various treatments that further changed their particle size (d) and surface chemisorbed oxygen (θ) [25]. The catalyst samples are divided in 8 sample sets based on their synthesis process and post-synthesis treatments (see Sect. 4.1).

2.2 Rate Constants of the Individual Reactions Steps

The rate data obtained from previous studies was collected at variable H_2O_2 concentration, reaction temperature and pH [17, 25, 26]. Briefly, the rate measurements were performed by adding 6 mg of a platinum nanocatalyst sample with known particle size and surface θ to an Erlenmeyer flask containing 1 L of H_2O_2 solution previously prepared at the desired conditions of, pH and T. The solution was sampled every 60 s for 5 min and the aliquots were used to determine the H_2O_2 concentration through a spectrophotometric method [17]. The initial rate method was used to determine the rate of H_2O_2 decomposition [30]. The H_2O_2 concentration was fit to a quadratic equation as function

Table 1 Notation used and units

$R_{H_2O_2}$	Initial rate of H_2O_2 decomposition, mol/m^2 s
$C_{H_2O_2}$	Concentration of H_2O_2, mol/L
t	Time, s
A	Pre-exponential constant in Arrhenius equation, mol/m^2 s
E_a	Activation energy, J/mol
R	Gas constant, 8.314 J/mol · K
T	Temperature, K
a_{H^+}	Activity of H^+ ion
k_i	Rate constant of reaction i, mol/m^2 · s
n_i	Reaction order for species i
R^2	Coefficient of determination for regression model
d	Particle size (diameter), nm
$O_{Pt(O)}$	Fraction of surface oxygen in the form of chemisorbed oxygen determined by XPS
S_O, S_{Pt}	Surface atomic fraction of oxygen or platinum, respectively, determined by XPS
$S_{Pt(O)}$	$O_{Pt(O)} \times S_O$, surface atomic fraction of chemisorbed oxygen
θ	$S_{Pt(O)}/(1/8 \cdot S_{Pt})$, fraction of catalyst surface covered with chemisorbed oxygen (Pt(O)) sites
$1-\theta$	Fraction of catalyst surface exposing metallic platinum (Pt) sites
v_i	Rate of reaction step i

of time and the slope of the curve at $t=0$ was used to determine the rate of H_2O_2 decomposition at each set of conditions.

The decomposition of H_2O_2 involves the oxidation of Pt to Pt(O) in the first step and its subsequent reduction to metallic Pt in the second step [17]. To determine the rate constants of the two reaction steps, we analyzed the kinetics of H_2O_2 decomposition on platinum surfaces with variable surface Pt(O)/Pt ratios. As the rate constant of a reaction depends on temperature through an Arrhenius relationship [31, 32], the analysis of the rate data was carried at the three tested experimental temperatures, 2 ± 2 °C, 21 ± 2 °C and 45 ± 5 °C [17, 18, 25, 26]. The rate data and surface θ for the entire sample set can be found in the supplemental information of Ref. [26]. The algebraic derivation to determine the rate constants of the individual steps is shown in Sect. 4. Table 1 gives the full notation list for the derivations shown in this work.

3 Results and Discussion

3.1 Properties of the Platinum Nanocatalysts

The platinum catalyst samples used for H_2O_2 decomposition rate data analysis in this study were previously characterized [25]. The rate data was normalized to the catalyst specific surface area to allow quantifying size induced effects on the catalytic activity. The fraction of catalyst surface covered with chemisorbed oxygen (θ) ranges from 0.21 to 0.69 for the entire sample set. Particle size and surface chemisorbed oxygen coverage of the original and treated nanocatalysts are shown in Table 2.

3.2 Rate Constants of the Individual Reaction Steps

The decomposition of H_2O_2 on platinum nanocatalysts is a two-step mechanism as represented by Eqs. 1, 2 and 3 [17].

Table 2 Particle size and surface θ of the platinum nanocatalyst samples used to measure the effect of these two variables on the rate of H_2O_2 decomposition. Adapted with permission from Ref. [26]

	Particle size	Surface θ
As received platinum black	8.80	0.21 ± 0.02
As received platinum nanopowder	19.9	0.66 ± 0.03
Platinum black heated in air	8.80–40.9	0.30–0.65
Platinum nanopowder heated in air	19.9	0.66 ± 0.02
Platinum black heated in vacuum	19.3	0.23 ± 0.01
Platinum nanopowder heated in vacuum	29.9	0.61 ± 0.02
Platinum black pre-treated with concentrated H_2O_2	8.80	0.39 ± 0.03
Platinum nanopowder pre-treated with concentrated H_2O_2	19.9	0.69 ± 0.02

$$\text{Step 1}\ \ Pt + H_2O_2 \rightarrow H_2O + Pt(O) \tag{1}$$

$$\text{Step 2}\ \ Pt(O) + H_2O_2 \rightarrow Pt + O_2 + H_2O \tag{2}$$

$$\text{Overall}\ \ 2H_2O_2 \rightarrow O_2 + 2H_2O \tag{3}$$

The overall rate of H_2O_2 decomposition on platinum nanocatalysts can be fit to a power law as function of H_2O_2 concentration, pH and surface θ (Eq. 7) [26, 32].

$$R_{H_2O_2} = \frac{-dC_{H_2O_2}}{dt} = k_3 \cdot \left(C_{H_2O_2}^{n_1}\right)\left(a_{H^+}^{n_2}\right)\left(\theta^{n_3}\right) \tag{4}$$

The effect of temperature in the reaction rate follows an Arrhenius relationship [30].

$$R_{H_2O_2} = \left(A \cdot e^{\frac{E_a}{R \cdot T}}\right)\left(C_{H_2O_2}^{n_1}\right)\left(a_{H^+}^{n_2}\right)\left(\theta^{n_3}\right) \tag{5}$$

The rate data considered in this study was fit to Eq. 5, which resulted in the following rate law for the overall reaction of H_2O_2 decomposition.

$$R_{H_2O_2} = 10^{2.87}\left(e^{\left(-\frac{(24.3\pm1.6)10^3}{R \cdot T}\right)}\right)\left(C_{H_2O_2}^{0.920\pm0.03}\right)\left(a_{H^+}^{0.037\pm0.01}\right)\left((\theta)^{0.828\pm0.03}\right) \tag{6}$$

where $k_3 = 10^{2.87}\left(e^{\left(-((24.3\pm1.6)10^3)/R \cdot T\right)}\right) = 0.0370$, at room temperature (T = 295 K).

As shown in Reaction 1, 2 and 3, the decomposition of H_2O_2 by platinum nanocatalysts is a multiple-step mechanism. Therefore, the rate constant of the overall reaction (k_3) reflects the combined effect of temperature on the rate constants of the multiple elementary steps of the H_2O_2 decomposition reaction [32, 33]. Therefore, the overall rate of H_2O_2 decomposition is given by the sum of the rate of H_2O_2 decomposition for step 1 (Eq. 1) and step 2 (Eq. 2). Thus, for a general case, Eq. 4 assumes the form of Eq. 7.

$$R_{H_2O_2} = \frac{-dC_{H_2O_2}}{dt} = k_3\left(\theta^{0.828}\right)\left(C_{H_2O_2}^{0.920}\right)\left(a_{H^+}^{0.037}\right)$$

$$R_{H_2O_2} = k_1(1-\theta)^{n_{3.1}}\left(C_{H_2O_2}^{0.920}\right)\left(a_{H^+}^{0.037}\right) + k_2(\theta)^{n_{3.2}}\left(C_{H_2O_2}^{0.920}\right)\left(a_{H^+}^{0.037}\right)$$

$$R_{H_2O_2} = \left(k_1(1-\theta)^{n_{3.1}} + k_2(\theta)^{n_{3.2}}\right)\left(C_{H_2O_2}^{0.920}\right)\left(a_{H^+}^{0.037}\right) \tag{7}$$

where $n_{3.1}$ and $n_{3.2}$ are the reaction order in terms of the surface catalyst sites in the metallic state $(1-\theta)$ and the surface catalyst sites with chemisorbed oxygen (θ), respectively.

Re-arranging this equation to obtain an equation with θ as the independent variable leads to

$$\frac{R_{H_2O_2}}{\left(C_{H_2O_2}^{n_1}\right)\left(a_{H^+}^{n_2}\right)} = \left(k_1(1-\theta)^{n_{3.1}} + k_2(\theta)^{n_{3.2}}\right) = (0.0370)\left(\theta^{0.828}\right) \tag{8}$$

And therefore,

$$\frac{k_1}{0.0370}(1-\theta)^{n_{3.1}} + \frac{k_2}{0.0370}(\theta)^{n_{3.2}} = \left(\theta^{0.828}\right) \tag{9}$$

For the case where step 1 and step 2 both have first order kinetics in terms of surface metallic platinum ($n_{3.1} = 1$) and surface sites with chemisorbed oxygen ($n_{3.2} = 1$), respectively, Eq. 9 can be simplified to Eq. 10.

$$\frac{k_1}{0.0370}(1-\theta)^1 + \frac{k_2}{0.0370}(\theta)^1 = \left(\theta^{0.828}\right)$$

$$\left(\theta^{0.828}\right) = \frac{\left(k_2 - k_1\right)}{0.0370}(\theta) + \frac{k_1}{0.0370} \tag{10}$$

where $((k_2 - k_1)/0.0370)$ and $k_1/0.0370$ are respectively the slope and the intercept of a linear regression that relates θ^{n_3} to θ. For the range of θ evaluated in the present study, at room temperature (T = 295 K), this linear regression is shown in Fig. 1.

The linear regression presented in Fig. 1 indicates that $k_1/0.0370 = 0.076$ and $(k_2 - k_1)/0.0370 = 0.964$, which results in $k_2 = 0.038$ mol/m$^2 \cdot$ s and $k_1 = 0.0028$ mol/m$^2 \cdot$ s for T = 295 K.

With the determined values of k_1 and k_2, the rate law for the overall reaction can be recast in terms of the intermediate reaction rate constants (Fig. 2, model 1).

$$R_{H_2O_2} = 0.0370\left(\theta^{0.83}\right)\left(C_{H_2O_2}^{0.920}\right)\left(a_{H^+}^{0.037}\right)$$

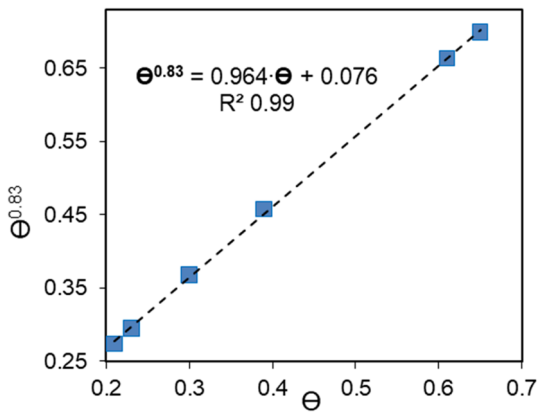

Fig. 1 Linear regression between θ^{n_3} and (θ) at T = 295 K for $0.21 < \theta < 0.69$

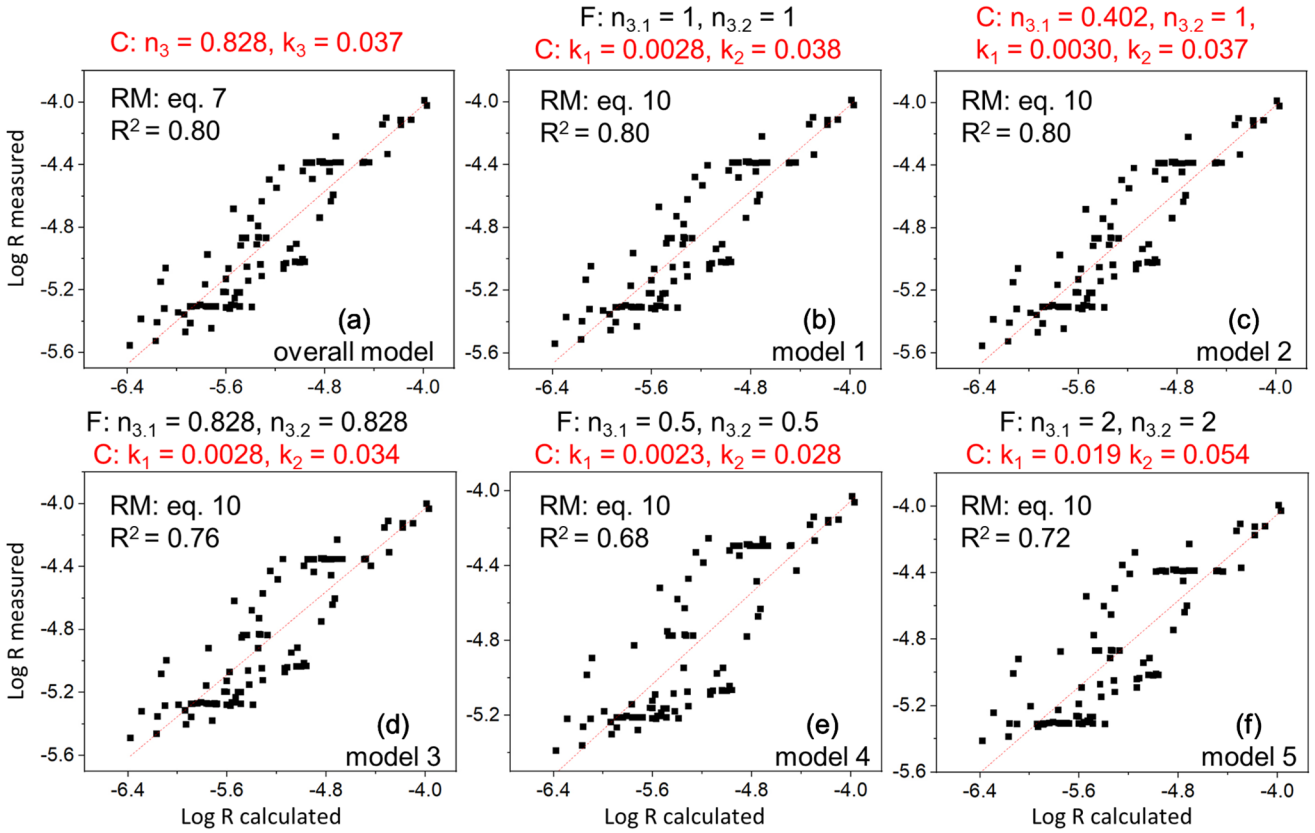

Fig. 2 Comparison of predicted and measured $\log R_{H_2O_2}$ for different reaction order scenarios in terms of surface sites with metallic Pt $(n_{3.1})$ and surface sites with chemisorbed oxygen $(n_{3.2})$. For each scenario, the variables in black were fixed (F:) and the variables in red were calculated (C:) using the module solver in excel to improve the fit of Eq. 4 (**a**) or Eq. 7 (**b**–**f**) to the experimentally measured R values

$$R_{H_2O_2} = (0.0028(1-\theta) + 0.038(\theta))\left(C_{H_2O_2}^{0.920}\right)\left(a_{H^+}^{0.037}\right) \quad (11)$$

For the cases where $n_{3.1} \neq 1$ and $n_{3.2} \neq 1$, the module solver was used to provide the values of k_1 and k_2 by fitting Eq. 7 to the measured rates of H_2O_2 decomposition. The effect of each variable on the rate of H_2O_2 decomposition can be linearized through a log transformation [30]. Figure 2 compares the log transformed rates of H_2O_2 decomposition to the rates calculated for models that consider different plausible values of $n_{3.1}$ and $n_{3.2}$ for rate measurements obtained at T = 295 K.

The results show that if both step 1 and step 2 are assumed to have first order kinetics in terms of $1-\theta$ and θ, respectively, the generated rate model has $R^2 = 0.80$ (model 1) (Fig. 2b). If the values of $n_{3.1}$ and $n_{3.2}$ are also allowed to be regressed, $n_{3.1}$ changes to 0.402 but the value of $n_{3.2}$ stays the same and equal to 1 (model 2). In this case $R^2 = 0.80$, which is the same as the R^2 value of model 1. Since the value of R^2 does not change, the small change observed in the value of $n_{3.1}$ from model 1 to model 2 is likely due to the uncertainty associated to the rate measurements. This indicates that the assumption that step 1 has first order kinetics in terms of $1-\theta$ and step 2 has first order kinetics in terms of θ is valid, which suggests that both step 1 and step 2 are elementary steps of the overall reaction mechanism [32, 34]. Model 1 and model 2 explain the variance of the measured data to the same extent as the model based on the overall reaction (overall model), which supports that the reaction mechanism shown in Eqs. 1, 2 and 3 is correct [17]. For comparison, we tested the effect of changing the values of $n_{3.1}$ and $n_{3.2}$ (Fig. 2d–f). If both $n_{3.1}$ and $n_{3.2}$ are set equal to $n_3 = 0.828$ and not allowed to be fit, the R^2 lowers to 0.76 (model 3). Likewise, if only one of these two values is imposed to be equal to n_3, while the other is left equal to 1, the R^2 of the obtained model is still significantly lower than that of model 1 (Figure S1). The R^2 value decreases even further if the values of $n_{3.1}$ and $n_{3.2}$ are decreased to 0.5 (model 4) or increased to 2 (model 5). Taken together our results indicate that the rate of H_2O_2 decomposition is appropriately described in terms of the intermediate reaction steps by Eq. 11 and at T = 295 K the rate constant of step 2 (k_2) is 14 times faster than that of step 1 (k_1), which corroborates that step 1 is the rate limiting step of the overall reaction [26].

The rate constants of the reaction are affected by temperature following an Arrhenius relationship $k = \mathrm{A} \cdot e^{-(E_a/R)(1/T)}$ [32, 33]. Equation 7 thus assumes the form of

$$R_{H_2O_2} = \left(A_1\left(e^{-\frac{(E_{a1})}{(R)(T)}}\right)(1-\theta)^{n_{3.1}} + A_2\left(e^{\frac{(E_{a2})}{(R)(T)}}\right)(\theta)^{n_{3.2}}\right)\left(C_{H_2O_2}^{0.920}\right)\left(a_{H^+}^{0.037}\right) \quad (12)$$

where $A_1\left(e^{-(E_{a1})/(R)(T)}\right) = k_1$ and $A_2\left(e^{(E_{a2})/(R)(T)}\right) = k_2$. Equation 12 has four unknown parameters A_1, A_2, E_{a1} and E_{a2}. From the analysis of the results at 295 K (Fig. 2) $n_{3.1}$ and $n_{3.2}$ are equal to 1. The four unknown parameters were determined by fitting Eq. 12 to the entire data set which included the rate measurements at 275 ± 2 K and 318 ± 5 K in addition to the measurements performed at room temperature (Fig. 3). The regression fit was further constrained by imposing that $k_2 = 0.038$ mol/m$^2 \cdot$ s and $k_1 = 0.0028$ mol/m$^2 \cdot$ s for T = 295 K as shown above. This additional constraint also prevented the system from reaching an unrealistic minimum, such as making $A_1 = 0$ and $A_2 = 2.87$, which would generate the same equation as that represented by the overall rate model (Eq. 6).

The results show that when all four parameters are allowed to be fit, the activation energy of step 1 is 4.4 times larger than that of step 2 (model 6). This is consistent with the fact that step 1 is the rate limiting step of the reaction and its rate constant at T = 295 K is 14 times slower than that of step 2. We compared the results obtained for model 6 with a model where E_{a1} and E_{a2} were imposed to be equal to 24,000 J•mol^{-1}, which is the activation energy associated to the overall reaction of H_2O_2 decomposition on platinum. This means that the difference in the rate constants of step 1 and step 2 would be entirely dictated by a different pre-exponential factor, which results in $A_1 = 63.1$ mol•m^{-2} and $A_2 = 794$ mol•m^{-2}. In this case the R^2 of the regression reduced from 0.79 to 0.76, which indicates that model 5 is a more reliable representation of the rate of H_2O_2 decomposition as function of temperature. Thus for a variable temperature Eq. 12 can be recast as

$$R_{H_2O_2} = \left(13.1 \cdot \left(e^{\left(-\frac{(20.1)10^3}{R \cdot T}\right)}\right)(1-\theta) + 0.29 \cdot \left(e^{\left(-\frac{(4.58)10^3}{R \cdot T}\right)}\right)(\theta)\right)\left(C_{H_2O_2}^{0.920}\right)\left(a_{H^+}^{0.037}\right)$$

This equation was used to calculate the values of k_1 and k_2 at the other experimental temperatures, T = 273 ± 2 K and T = 318 ± 5 (Table 3).

The difference between the rate constant of step 1 and step 2 decreases with temperature because the effect of temperature is stronger on step 1 (larger activation energy). Step 2 is 20 times faster than step 1 at T = 275 but their difference drops to only 8 times at T = 318 K. Figure 4 shows the effect of temperature on the rate constants of step 1 and step 2 in the range of temperatures evaluated in this study.

The rate of step 1 increases faster than that of step 2 as the temperature increases. That means that temperature has a double effect on the overall rate of H_2O_2 decomposition catalyzed by platinum. On one hand it increases the individual rates of step 1 and step 2. On the other hand it allows the rate of step 1 (the rate limiting step of the reaction) to approach that of step 2.

Table 3 Rate constants of the overall (k_3) and elementary reaction steps (k_1 and k_2) at the tested experimental temperatures

Temperature (K)	k_1	k_2	k_3
273	0.0020	0.039	0.0166
295	0.0028	0.038	0.0370
318	0.0065	0.051	0.0756

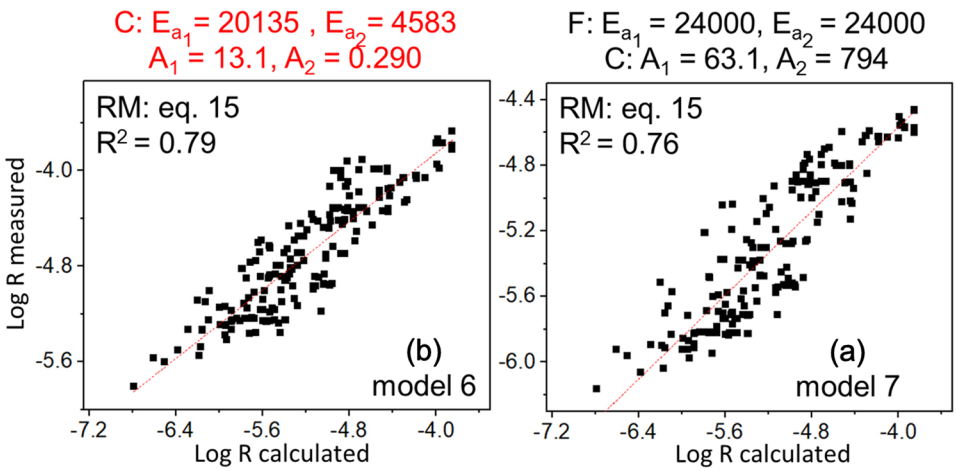

Fig. 3 Comparison of predicted and measured log $R_{H_2O_2}$ for different pre-exponential (A) and activation energy (E_a) scenarios for both step 1 and step 2 of the H_2O_2 decomposition reaction. For each scenario, the variables in black were fixed (F:) and the variables in red were calculated (C:) using the module solver in excel to improve the fit of Eq. 12 to the experimentally measured R values at all tested reaction temperatures

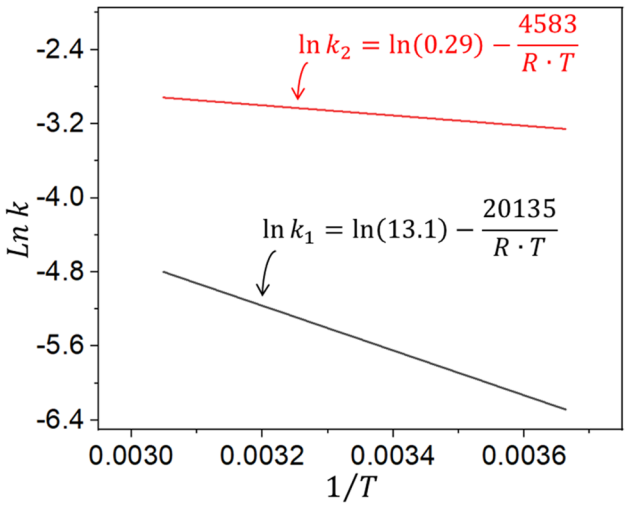

Fig. 4 Arrhenius relationship of k_1 and k_2 with temperature

3.3 Role of Chemisorbed Oxygen on Catalytic Activity of H_2O_2 Decomposition by Platinum

Our results show that the surface θ of each sample affects the initial rate of H_2O_2 decomposition, particularly at low temperatures. This is important because the abundance of surface sites with chemisorbed oxygen varies for different platinum nanocatalyst samples (Table 2). Because the relative rates of step 1 and step 2 are different, surface θ changes while platinum catalyzes H_2O_2 decomposition until steady state is reached. After steady state is reached the rate of step 2 becomes limited by the rate at which surface Pt(O) sites are formed (step 1) [19, 35]. Therefore, at steady state

$$v_1 = v_2 \tag{13}$$

$$k_1(1-\theta)C_{H_2O_2} = k_2\theta C_{H_2O_2} \tag{14}$$

$$\frac{\theta}{1-\theta} = \frac{k_1}{k_2} \tag{15}$$

As shown in Eq. 15, after steady state is reached the ratio of $\theta/1-\theta$ (ratio of catalyst surface covered with Pt(O) to catalysts surface covered with metallic Pt) at the nanocatalysts surface depends uniquely on the ratio of the rate constants of step 1 and step 2. This is important because chemisorbed oxygen is more stable on larger platinum nanoparticles compared to smaller ones [36–39]. That means that when steady state is reached, larger particles will have a larger fraction of the surface covered with surface chemisorbed oxygen, and therefore their rate of H_2O_2 decomposition is also faster, regardless of their original surface θ values. This is consistent with the fact that the surface θ of Pt nanopowder pre-treated with H_2O_2 (d = 19.9 nm) is 1.77 times higher than that of Pt black pre-treated with H_2O_2 (d = 8.80 nm) (Table 2). Given that step 1 is the rate limiting step of the reaction, from Eq. 15 we can conclude that in steady state the overall reaction rate model can be represented by Eq. 16.

$$R_{H_2O_2} = \frac{-dC_{H_2O_2}}{dt} = 2 \cdot k_1(1-\theta)\left(C_{H_2O_2}^{0.92}\right)\left(a_{H^+}^{0.04}\right)$$

$$R_{H_2O_2} = 2 \times 13.1 \times \left(e^{\left(-\frac{(20.1)10^3}{R \cdot T}\right)}\right)(1-\theta)\left(C_{H_2O_2}^{0.92}\right)\left(a_{H^+}^{0.04}\right) \tag{16}$$

The model shown in Eq. 16 indicates that when steady state is reached the overall rate of H_2O_2 decomposition is twice the rate of H_2O_2 decomposition through reaction step 1. Reaction step 2 is responsible for most of the H_2O_2 decomposed in the initial moments of reaction for samples with high surface θ, but the rate of this step becomes limited by the rate of step 1 as soon as steady state surface θ coverage is reached.

These results quantify for the first time the relative rate of H_2O_2 decomposition of the two intermediate reactions steps and corroborates the fundamental role of surface Pt(O) for controlling the overall rate of H_2O_2 decomposition on platinum nanocatalysts. It reconciles previous studies that reported induction periods of H_2O_2 decomposition on freshly exposed platinum surfaces [27, 39], while enhanced rates were observed for samples subjected to cold-working or heated in open atmospheric conditions [24]. This information can be used to engineer both the catalyst properties and reaction conditions toward controlling the rate at which H_2O_2 is decomposed. For example, by applying an electric bias it is possible to change the fraction of the catalyst surface covered with Pt(O) sites, which has the potential to increase the rate of H_2O_2 decomposition by a factor of 14 at room temperature [21]. Likewise, the rate limiting effects of step 1 can be reduced by using a higher reaction temperature. These results have the potential to improve industrial and technological applications that depend on the rate of H_2O_2 decomposition catalyzed by platinum, such as thrust generation on spacecraft jets and hydrogen fuel cells [1–3, 40].

4 Conclusions

Hydrogen peroxide decomposition on platinum is a cyclic reaction where Pt oxidizes to Pt(O) and reduces back to Pt. This work shows for the first time that the overall rate of H_2O_2 decomposition on platinum nanocatalysts can be significantly increased by controlling the accumulation of chemisorbed oxygen at the catalyst surface. Step 1, the oxidation of Pt → Pt(O), is the rate limiting step of the

reaction. The rate of step approaches that of step 2 for higher reaction temperature. At steady state the overall rate of reaction is twice the rate of step 1 because the two steps happen sequentially. These results are important for improving the efficiency of platinum nanocatalysts used in technological and industrial applications, such as hydrogen fuel cells and hydrogen peroxide synthesis. In addition, the methodology presented in this study can also be used to calculate the individual rate constants of many other chemical reactions where the catalyst surface cycles through two oxidation states. This will lead to improved understanding of how reaction conditions and catalyst properties can be engineered to optimize catalysis reactions in different industrial and technological processes.

Acknowledgements F. M. M. and R. S. M. gratefully acknowledge financial support from the Virginia Tech Institute for Critical Technology and Applied Science (ICTAS) through a Junior Faculty Collaborative Grant (ICTAS-JFC 175884) and the Virginia Tech National Center for Earth and Environmental Nanotechnology "NanoEarth" funded by the National Science Foundation (NNCI-1542100). R. S. M. gratefully acknowledges the Virginia Tech College of Science Roundtable Alumni Advisory Group for financial support provided through a "Make-a-Difference" Scholarship, as well as the Department of Geosciences for support provided by Sir Aubrey and Madam Eula Orange Scholarship funds. The authors also thank Dr. Robert Bodnar and Mr. Charles Farley for support with selected experiments.

Compliance with Ethical Standards

Conflict of interest The authors declare that they have no conflict of interest.

References

1. Chen B, Garland NT, Geder J, Pruessner M, Mootz E, Cargill A et al (2016) Platinum nanoparticle decorated SiO_2 microfibers as catalysts for micro unmanned underwater vehicle propulsion. ACS Appl Mater Interfaces 8(45):30941–30947
2. Krejci D, Woschnak A, Scharlemann C, Ponweiser K (2012) Structural impact of honeycomb catalysts on hydrogen peroxide decomposition for micro propulsion. Chem Eng Res Des 90(12):2302–2315
3. Marr KM, Chen B, Mootz EJ, Geder J, Pruessner M, Melde BJ et al (2015) High aspect ratio carbon nanotube membranes decorated with Pt nanoparticle urchins for micro underwater vehicle propulsion via H_2O_2 decomposition. ACS Nano 9(8):7791–7803
4. He F, Tang Y, Yu M, Wang S, Li Y, Zhu D (2006) Fluorescence-amplifying detection of hydrogen peroxide with cationic conjugated polymers, and its application to glucose sensing. Adv Funct Mater 16(1):91–94
5. Pickup JC (1993) In vivo glucose monitoring: sense and sensorbility. Diabetes Care 16(2):535–539
6. Wu P, He Y, Wang H-F, Yan X-P (2010) Conjugation of glucose oxidase onto Mn-doped ZnS quantum dots for phosphorescent sensing of glucose in biological fluids. Anal Chem 82(4):1427–1433
7. Tamao K, Kumada M, Maeda K (1984) Silafunctional compounds in organic synthesis. 21. Hydrogen peroxide oxidation of alkenyl(alkoxy)silanes. Tetrahedron Lett 25(3):321–324
8. Legros J, Bolm C (2003) Iron-catalyzed asymmetric sulfide oxidation with aqueous hydrogen peroxide. Angew Chem Int Ed 42(44):5487–5489
9. Hammerschmidt A, Domke WD, Nolscher C, Suchy P (2000). PEM fuel cell. Google Patents
10. Li Y, Yang J, Song J (2017) Structure models and nano energy system design for proton exchange membrane fuel cells in electric energy vehicles. Renew Sustain Energy Rev 67:160–172
11. Nie Y, Li L, Wei Z (2015) Recent advancements in Pt and Pt-free catalysts for oxygen reduction reaction. Chem Soc Rev 44(8):2168–2201
12. Campos-Martin JM, Blanco-Brieva G, Fierro JLG (2006) Hydrogen peroxide synthesis: an outlook beyond the anthraquinone process. Angew Chem Int Ed 45(42):6962–6984
13. Edwards JK, Freakley SJ, Carley AF, Kiely CJ, Hutchings GJ (2013) Strategies for designing supported gold–palladium bimetallic catalysts for the direct synthesis of hydrogen peroxide. Acc Chem Res 47(3):845–854
14. Panchanathan D, Rajappan A, Varanasi KK, McKinley GH (2018) Plastron regeneration on submerged superhydrophobic surfaces using in situ gas generation by chemical reaction. ACS Appl Mater Interfaces 10(39):33684–33692
15. Li Y, Yun K-H, Lee H, Goh S-H, Suh Y-G, Choi Y (2019) Porous platinum nanoparticles as a high-Z and oxygen generating nanozyme for enhanced radiotherapy in vivo. Biomaterials 197:12–19
16. Zhao K, Zhuang S, Chang Z, Songm H, Dai L, He P et al (2007) Amperometric glucose biosensor based on platinum nanoparticles combined aligned carbon nanotubes electrode. Electroanalysis 19(10):1069–1074
17. Serra-Maia R, Bellier M, Chastka S, Tranhuu K, Subowo A, Rimstidt JD et al (2018) Mechanism and kinetics of hydrogen peroxide decomposition on platinum nanocatalysts. ACS Appl Mater Interfaces 10(25):21224–21234
18. Serra Maia RF (2018) Relation between surface structural and chemical properties of platinum nanoparticles and their catalytic activity in the decomposition of hydrogen peroxide: Virginia Tech
19. Bianchi G, Mazza F, Mussini T (1962) Catalytic decomposition of acid hydrogen peroxide solutions on platinum, iridium, palladium and gold surfaces. Electrochim Acta 7(4):457–473
20. Eley DD, Macmahon DM (1972) The decomposition of hydrogen peroxide catalysed by palladium-gold alloy wires. J Colloid Interface Sci 38(2):502–510
21. Hall SB, Khudaish EA, Hart AL (1998) Electrochemical oxidation of hydrogen peroxide at platinum electrodes. Part II: effect of potential. Electrochim Acta 43(14):2015–2024
22. Roy CB (1968) Catalytic decomposition of hydrogen peroxide on some oxide catalysts. J Catal 12(2):129–133
23. Weiss J (1935) The catalytic decomposition of hydrogen peroxide on different metals. Trans Faraday Soc 31:1547–1557
24. Garwig PL (1966) Heterogeneous decomposition of hydrogen peroxide by inorganic catalysts. A literature survey. Princeton, FMC CORP
25. Serra-Maia R, Winkler C, Murayama M, Tranhuu K, Michel FM (2018) Abundance and speciation of surface oxygen on nanosized platinum catalysts and effect on catalytic activity. ACS Appl Energy Mater 1:3255–3266
26. Serra-Maia R, Chastka S, Bellier M, Douglas T, Rimstidt JD, Michel FM (2019) Effect of particle size on catalytic decomposition of hydrogen peroxide by platinum nanocatalysts. J Catal 373:58–66

27. Eley D, MacMahon D (1972) The decomposition of hydrogen peroxide catalysed by palladium-gold alloy wires. J Colloid Interface Sci 38(2):502–510
28. Stanca SE, Hänschke F, Ihring A, Zieger G, Dellith J, Kessler E et al (2017) Chemical and electrochemical synthesis of platinum black. Sci Rep 7:1074
29. Larminie J, Dicks A (2003) Fuel Cell Systems explained. Wiley, New York
30. Rimstidt JD (2014) Geochemical rate models: an introduction to geochemical kinetics. Cambridge University Press, Cambridge
31. Rimstidt JD (2013) Geochemical rate models: an introduction to geochemical kinetics. Cambridge University Press, Cambridge
32. Lente G (2015) Deterministic kinetics in chemistry and systems biology: the dynamics of complex reaction networks. Springer, New York
33. Jencks WP (1987) Catalysis in chemistry and enzymology. Courier Corporation, Chelmsford
34. Di Giacomo F (2015) A short account of RRKM theory of unimolecular reactions and of marcus theory of electron transfer in a historical perspective. J Chem Educ 92(3):476–481
35. McKee DW (1969) Catalytic decomposition of hydrogen peroxide by metals and alloys of the platinum group. J Catal 14(4):355–364
36. Kinoshita K (1990) Particle size effects for oxygen reduction on highly dispersed platinum in acid electrolytes. J Electrochem Soc 137(3):845–848
37. Trasatti S (1972) Electronegativity, work function, and heat of adsorption of hydrogen on metals. J Chem Soc Faraday Trans 68:229–236
38. Mason MG (1983) Electronic structure of supported small metal clusters. Phys Rev B 27(2):748–762
39. Zhou L, Zachariah MR (2012) Size resolved particle work function measurement of free nanoparticles: aggregates vs. spheres. Chem Phys Lett 525–526:77–81
40. Balasubramanian B, Barbir F, Neutzler J (1999) Optimal operating temperature and pressure of PEM fuel cell systems in automotive applications

Affiliations

Rui Serra-Maia[1] · J. Donald Rimstidt[2] · F. Marc Michel[2]

[1] Department of Materials Sciences Engineering, University of Pennsylvania, Philadelphia, PA 19104, USA

[2] Department of Geosciences, Virginia Polytechnic Institute and State University, Blacksburg, VA 24061, USA